ACS APPLIED MATERIALS & INTERFACES

www.acsami.org

Research Article

Additive Manufacturing of Optical Quality Germania–Silica Glasses

Koroush Sasan,* Andrew Lange, Timothy D. Yee, Nikola Dudukovic, Du T. Nguyen, Michael A. Johnson, Oscar D. Herrera, Jae Hyuck Yoo, April M. Sawvel, Megan Elizabeth Ellis, Christopher M. Mah, Rick Ryerson, Lana L. Wong, Tayyab Suratwala, Joel F. Destino, and Rebecca Dylla-Spears

Cite This: *ACS Appl. Mater. Interfaces* 2020, 12, 6736–6741

Read Online

ACCESS | Metrics & More | Article Recommendations | Supporting Information

ABSTRACT: Direct ink writing (DIW) three-dimensional (3D) printing provides a revolutionary approach to fabricating components with gradients in material properties. Herein, we report a method for generating colloidal germania feedstock and germania–silica inks for the production of optical quality germania–silica (GeO_2–SiO_2) glasses by DIW, making available a new material composition for the development of multimaterial and functionally graded optical quality glasses and ceramics by additive manufacturing. Colloidal germania and silica particles are prepared by a base-catalyzed sol–gel method and converted to printable shear-thinning suspensions with desired viscoelastic properties for DIW. The volatile solvents are then evaporated, and the green bodies are calcined and sintered to produce transparent, crack-free glasses. Chemical and structural evolution of GeO_2–SiO_2 glasses is confirmed by nuclear magnetic resonance, X-ray diffraction, and Raman spectroscopy. UV–vis transmission and optical homogeneity measurements reveal comparable performance of the 3D printed GeO_2–SiO_2 glasses to glasses produced using conventional approaches and improved performance over 3D printed TiO_2–SiO_2 inks. Moreover, because GeO_2–SiO_2 inks are compatible with DIW technology, they offer exciting options for forming new materials with patterned compositions such as gradients in the refractive index that cannot be achieved with conventional manufacturing approaches.

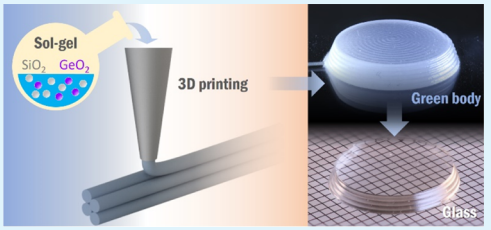

KEYWORDS: *3D printing, GeO_2–SiO_2 glass, sol–gel, multimaterial, direct ink writing*

1. INTRODUCTION

Glass is an ideal material for many optical applications because of its properties such as high chemical and temperature resistance and transparency.[1−3] The utility and function within an optical system of a particular glass is significantly impacted by its refractive index.[4,5] Thus, control of the refractive index across and within optical materials is critical for producing suitable glass materials for advanced optical systems. For example, using a high refractive index glass can allow for less optical components, thus saving weight, while maintaining similar or better imaging angles and quality.[6] The refractive index can be modified by adding alloying components, such as ZrO_2, TiO_2, and GeO_2, to silica to produce binary glasses with greater refractive indices.[6,7] These optical glasses are typically formed by melting constituent glass oxides together, which require high temperatures and multiple processing steps for production.[8]

The rise of additive manufacturing has allowed access to a larger design space through higher tunability of material properties and geometries.[9−12] As such, these expanded capabilities have driven research efforts to develop optics with novel geometries and/or tailored optical properties, such as a spatially varying refractive index fabricated through material composition variation.[10] Although glass is highly desired for such applications, work in additive manufacturing of such a material is still in the early stages.

Previous studies have reported different routes to additively manufacture glass, typically through selectively depositing a molten material via laser melting or a melted filament.[6,13−15] In some cases, the resulting glass suffers from low optical quality or lack of transparency, making them poor alternatives to conventionally produced glass, as the melting process causes steep thermal gradients which degrade the refractive index homogeneity of the material. These processes also have sourced feedstock materials from either commercial fumed silica or conventional melt-glass processes, with demonstrations in transparent silica glass,[6] fused quartz,[15] and soda-lime glass.[13] Importantly, none of these three-dimensional (3D) printing methods is readily adaptable to either rapid material switching or feedstock blending required for producing compositionally graded or patterned components such as gradient index optical glass.

Received: November 20, 2019
Accepted: January 14, 2020
Published: January 14, 2020

https://dx.doi.org/10.1021/acsami.9b21136
ACS Appl. Mater. Interfaces 2020, 12, 6736–6741

We have recently reported an alternate method to 3D printing optical quality silica−titania glass via direct ink writing (DIW).[3,10,16] To briefly describe this method, a shear-thinning ink is formulated from a colloidal silica suspension and extruded from a tip, allowing for a 3D shape to be printed filament by filament. Once the print is complete, it is then heat-treated and sintered to form transparent glass. When the DIW system is equipped with an inline mixer, multiple inks can be blended in varying ratios to create gradient composition components.[17]

A key challenge in the development of gradient index optical glasses by DIW is formulating inks with the various dopants needed to achieve a target glass property such as refractive index that can also be blended with compatible inks.[3,10] The addition of a dopant species with different characteristics such as size, morphology, or chemistry may dramatically affect the ink's printability, thermal processing conditions, or optical quality. Therefore, the development of a robust and tunable set of feedstocks for glass 3D printing will not only enable greater variety and flexibility in achieving desirable glass with gradient properties but will also lead to a better understanding of the roles these factors play in glass ink formulation.

Here, we demonstrate the first optical quality germania−silicate (GeO_2−SiO_2) glasses fabricated by 3D printing. We detail a route to the production of colloidal germania feedstock particles amenable to blending with silica colloids in various compositions to change the refractive index. We describe the process by which the colloidal particles are converted to inks, printed by DIW, and then converted to glasses with varying germania concentrations. Finally, we characterize the printed GeO_2−SiO_2 glasses to show they are comparable to those prepared by conventional methods (i.e., sol−gel and melting) in terms of network structure, chemical composition, optical transmission, and refractive index.

2. EXPERIMENTAL SECTION

2.1. Sample Preparation. The silica and germania sols used in this study were prepared by the sol−gel method as described elsewhere.[3] A typical GeO_2−SiO_2 ink was prepared by blending silica sol with the desired molar ratio of the germania sol. The EtOH solvent and residual H_2O were then exchanged using a rotary evaporator with 2-[(2-methoxyethoxy)ethoxy]acetic acid, 1-hexanol, propylene carbonate (PC), and tetraglyme (TG). The resulting GeO_2−SiO_2 inks were then mixed by a planetary centrifugal mixer for 60 s at 2200 rpm. To determine the solids content of the inks, aliquots were dried at 300 °C for 12 h. The solids were then adjusted to the appropriate concentration with PC and mixed for 2 min at 2200 rpm. The final inks have a solids loading of 30 wt % and are stable for approximately 1 week in a sealed container. The inks were printed using a DIW setup, as described elsewhere.[3]

2.2. Characterization. The composition and structure of the samples were determined using electron microprobe microanalysis (EPMA), Rutherford backscattering spectrometry (RBS), Raman spectroscopy, and nuclear magnetic resonance (NMR). More details about these characterization techniques are provided in the Supporting Information.

3. RESULTS AND DISCUSSION

The GeO_2−SiO_2 sol−gel inks are prepared via three steps, as shown in Figure 1. First, SiO_2 and GeO_2 particles are separately prepared by the sol−gel method by mixing either tetraethyl orthosilicate or germanium(IV) ethoxide in EtOH with H_2O and ammonia, which serve as catalysts. Both the GeO_2 and the SiO_2 particles reach steady-state radius

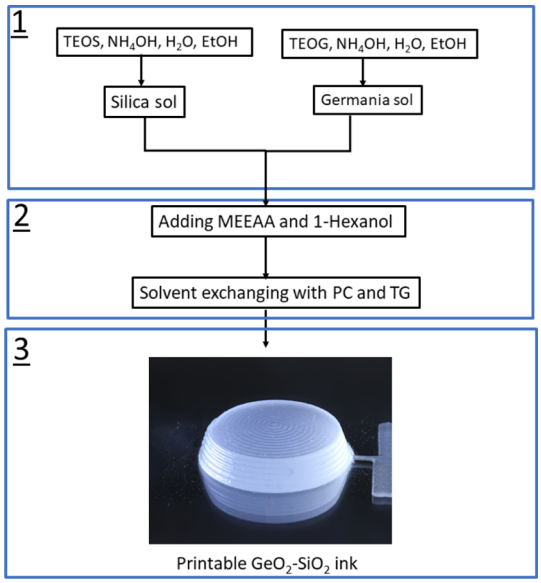

Figure 1. GeO_2−SiO_2 ink preparation process scheme.

distributions of 18.5 ± 1.5 nm (see Figure S1) within approximately 7 days.

Next, the SiO_2 and GeO_2 particle sols are blended together in the molar ratio desired for the final glass. 2-[(2-Methoxyethoxy)ethoxy]acetic acid and 1-hexanol are also added to the premixed sol solutions to improve stability in the final ink by preventing particle agglomeration.[3]

Finally, the GeO_2−SiO_2 sols are transformed into inks. The low vapor pressure solvents PC and TG are added to the premixed sol. EtOH and H_2O are subsequently removed using rotary vacuum evaporation. PC and TG have been shown to help control the rheological properties of the ink during printing as well as the drying rates during consolidation.[3] The resulting GeO_2−SiO_2 inks are stable for 1 week.

The rheological behavior of 2.5, 5, and 7.5% GeO_2−SiO_2 inks is shown in Figure 2. All inks were formulated with a

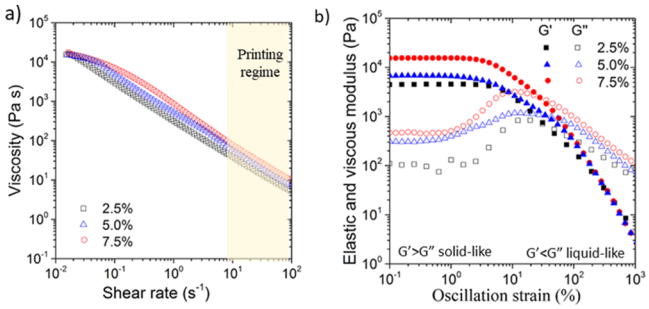

Figure 2. (a) Rheological flow curves of 2.5, 5.0, and 7.5% (mol %) of GeO_2−SiO_2 inks under steady shear. (b) Viscoelastic properties of GeO_2−SiO_2 inks.

solids loading of 30 wt %. This allowed the inks to have consistent flow properties while limiting shrinkage during sintering. The final GeO_2−SiO_2 inks exhibit pronounced shear-thinning behavior, which facilitates flow through the nozzle during printing. The viscosity and elastic moduli of the inks increase slightly with increasing GeO_2 content (see Figure 2a,b), but all inks exhibit a similar shear-thinning behavior within the same order of magnitude. Figure 2b indicates linear elastic-dominated (solid-like) behavior in the inks up to

https://dx.doi.org/10.1021/acsami.9b21136
ACS Appl. Mater. Interfaces 2020, 12, 6736−6741

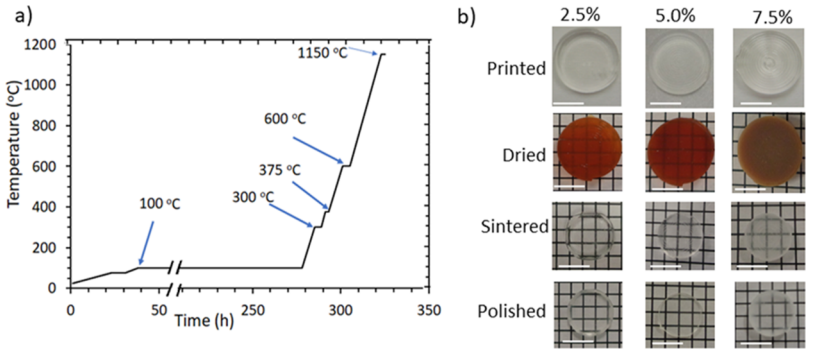

Figure 3. (a) Thermal processing schedule of GeO_2−SiO_2 printed parts. (b) DIW sol−gel and 2.5, 5, and 7.5% (mol %) GeO_2−SiO_2 glass components at various stages of the heat treatment. The scale bar is 5 mm in all images.

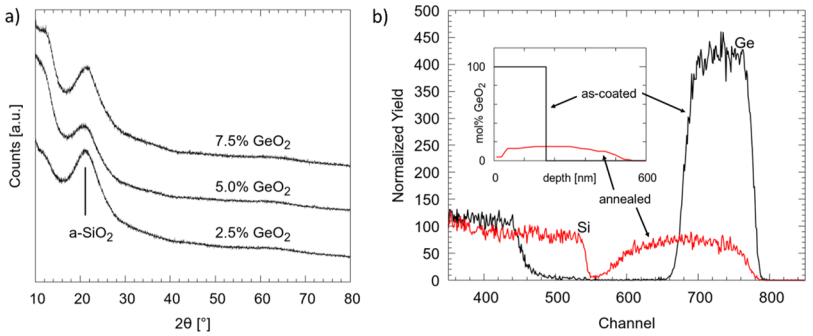

Figure 4. (a) XRD patterns of the 2.5, 5, and 7.5% (mol %) GeO_2−SiO_2 glass samples. (b) RBS analysis of GeO_2 coating on SiO_2 glass before (as-deposited) and after thermal annealing (annealed) at 1150 °C for 91 h. The inset in (b) shows composition profile extracted by fitting RBS data.

oscillation strains of around 1% ($G' > G''$), followed by nonlinear deformation yielding around 10% strain ($G' < G''$, indicative of flow), allowing the ink to be printed at modest pressures. During printing, the particle network is quickly reformed, which allows rapid elastic recovery and fast resolidification after the inks exit the nozzle (see Figure S2). Moreover, the rheology of the GeO_2−SiO_2 inks is designed to match the behavior of previously reported SiO_2 and TiO_2−SiO_2 inks.[3] Ensuring similar elastic moduli and yield stresses between different inks (see Figure S3) allows for the possibility of coprinting multiple materials at once with the same extrusion parameters and avoiding the pitfalls of unmatched postextrusion behavior. In addition, the ability to print a single structure from multiple inks with matching solids loading enables the subsequent coprocessing through thermal treatment, giving rise to a path to multimaterial glasses with a spatial change in the refractive index.[10]

The GeO_2−SiO_2 inks are printed by DIW into cylinders of a single composition. The green bodies then undergo the heat treatment process shown in Figure 3 to produce GeO_2−SiO_2 glass. First, the green bodies are dried at 100 °C to increase the strength of the green body without forming cracks. Next, the monoliths are calcined between 300 and 600 °C, removing organic components. Finally, the calcined parts are sintered into transparent glass.

The drying process is critical for producing a crack-free monolith as the capillary forces produce shrinkage stresses, especially at fast evaporation rates.[18−20] To mitigate this issue, the printed parts are dried slowly over 10 days at 100 °C. The remaining low vapor pressure solvents are then removed by increasing the temperature to 375 °C (see Figure S4). The temperature is then increased to 600 °C for 4 h to burn out the remaining organics. Without the burnout process, the organic components can remain in the glass which results in opacity after full densification. After burnout, the printed parts are densified at 1150 °C in air for 2 h to achieve GeO_2−SiO_2 glass with no cracks. In Figure 3b, photographs of polished, fully dense, and transparent 2.5 and 5% GeO_2−SiO_2 glasses are shown. The 7.5% GeO_2−SiO_2 glass appeared cloudy because of the phase separation of GeO_2 during the sintering process (see Figure S5).[21,22] An electron microprobe analyzer was used to evaluate the chemical composition of the GeO_2−SiO_2 glasses after sintering, which showed that no germania was lost from sintering (see Figure S6).

Solid-state ^{29}Si magic angle spinning NMR and Q-species analysis was carried out for both the printed and commercial (Corning 7980) glasses to compare the bonding environment of Si. Q-species analysis shows (see Figure S7) that all samples are nearly identical with 100% Q^4 speciation, which indicates that DIW GeO_2−SiO_2 glasses are fully dense (Q^4) networks and compare well with the fused silica standard, Corning 7980.[3]

Figure 4a shows the results of X-ray diffraction (XRD) θ−2θ measurements, which were carried out in Bragg−Brentano geometry. The absence of sharp peaks in the fully dense samples containing 2.5, 5, and 7.5% GeO_2 (Figure 4a) suggests that the samples did not undergo crystallization during the thermal treatment. As indicated, these samples showed only a broad peak associated with amorphous SiO_2.

The interdiffusion of germania and silica at the sintering temperature was also investigated. First, a thin film (~200 nm) of sol−gel-derived GeO_2 was dip-coated onto a fused silica wafer (Corning 7980). The as-coated sample was then annealed for 1 h at 1000 °C to presinter the sample. The Ge

https://dx.doi.org/10.1021/acsami.9b21136
ACS Appl. Mater. Interfaces 2020, 12, 6736−6741

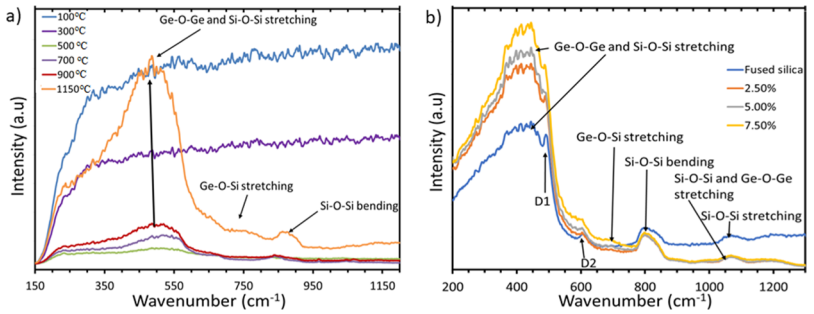

Figure 5. (a) Room-temperature Raman spectra of the 5% GeO_2−SiO_2 ink collected after different stages of heat treatment. (b) Raman spectra of the Corning 7980 and DIW 2.5, 5, and 7.5% GeO_2−SiO_2 glasses recorded at room temperature.

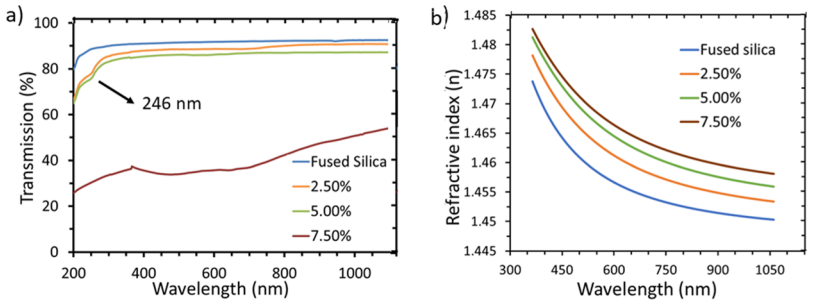

Figure 6. (a) UV−vis optical transmission spectra of commercial fused silica (uncoated) and DIW 2.5, 5.0, and 7.5% GeO_2−SiO_2 glasses over 200−1100 nm. (b) Optical dispersion measurements of commercial fused silica and DIW 2.5, 5.0, and 7.5% GeO_2−SiO_2 glasses.

composition profiles were measured both after presintering and after annealing at 1150 °C for 91 h using RBS, as shown in Figure 4b. Here, the RBS signal from the as-coated sample is shown in black and the signal from the annealed sample is shown in red. The diffusion coefficient for Ge was previously found to be ∼2 × 10^{-16} cm^2/s when Ge was ion-implanted into SiO_2.[23−26] Based on this value for solid-state diffusion, one would expect the diffusion tail of Ge into the SiO_2 wafer to have a breadth of $\sim 2\sqrt{Dt} \approx 161$ nm. However, the concentration of GeO_2 in this experiment decreased to ∼15 mol % and extended ∼400 nm into the substrate as shown by the concentration profiles in the inset of Figure 4b. This indicates that GeO_2 melts at 1150 °C and dissolves into the adjacent SiO_2 until the solidus concentration is reached, which is then followed by rapid diffusion of Si into GeO_2 (relative to the expected rates of Ge diffusion in SiO_2). Therefore, the GeO_2−SiO_2 green bodies undergo liquid phase sintering under the conditions used in this system.

To investigate bond formation during sintering, we acquired Raman spectra of 5% GeO_2−SiO_2 ink samples heat-treated at various temperatures (Figure 5a). The Raman spectra of the green bodies heat-treated at temperatures between 100 and 500 °C are dominated by a broad photoluminescent peak, likely caused by organic components in the ink, such as PC and TG (see Figure S8). During the burnout process above 600 °C, the organic components are volatilized, and the stretching modes of Ge−O−Ge and Si−O−Si and the Si−O−Si bonds can be seen.[27] Furthermore, when the green body is sintered at 1150 °C, the presence of the Ge−O−Si band at ∼683 cm^{-1} is observed. This is a characteristic of binary GeO_2−SiO_2 glasses.[27,28]

The Raman spectrum of SiO_2 and printed GeO_2−SiO_2 glasses with different Ge concentrations is also shown in Figure 5b to highlight the concentration dependence of the sintering process. The Raman spectrum of binary GeO_2−SiO_2 mixed glasses shows several changes relative to pure SiO_2 glass. A peak at ∼683 cm^{-1} was observed in the binary glasses because of modes associated with Ge−O−Si bonds.[27,29] The sharp D1 and D2 defect bands of the SiO_2 glass decrease in intensity with increasing dopant content.[28−30] The decreasing intensity of defect bands (D1 and D2) suggests that the four-membered rings of SiO_2 tetrahedra become unstable with the addition of Ge.[29] Si−O−Si symmetric stretching is observed, as evidenced from the 430 cm^{-1} band, where the bandwidth and frequency are lower with increasing germania content, indicating that the addition of the dopant alters the network structure through decreasing the average atomic bond angle.[27,29]

Figure 6a shows optical transmission spectra for commercial fused silica and DIW 2.5, 5.0, and 7.5% GeO_2−SiO_2 glasses over wavelengths from 200 to 1100 nm. The 2.5 and 5% GeO_2−SiO_2 glasses show a shoulder absorption peak at 246 nm, which is associated with amorphous GeO_2. In addition, the shape of the spectra for the DIW 2.5 and 5% GeO_2−SiO_2 glasses compares well with that of fused silica, transmitting greater than ∼85% across the visible spectrum. The DIW 7.5% GeO_2−SiO_2 glass, which is visually less transparent (Figure 3b), shows substantially reduced transmission (∼25%) compared to that of the fused silica. All compositions exhibited a band edge cutoff similar to that of fused silica (∼200 nm), representing a distinct advantage over previously demonstrated 3D printed TiO_2−SiO_2 glasses (cutoffs at 260 and 365 nm) for applications in UV.[3] Figure 6b shows optical dispersion curves of fused silica and DIW 2.5, 5.0, and 7.5% GeO_2−SiO_2 glasses. As expected, the refractive index of the GeO_2−SiO_2 glass increases with increasing GeO_2 content. The glasses with higher GeO_2 are also more dispersive. This is consistent with the variation in absorption edges shown in Figure 6a. The observed refractive indices and corresponding Abbe numbers ($V_d \cong 60$) of DIW GeO_2−SiO_2 glasses (see Table S1) are

https://dx.doi.org/10.1021/acsami.9b21136
ACS Appl. Mater. Interfaces 2020, 12, 6736−6741

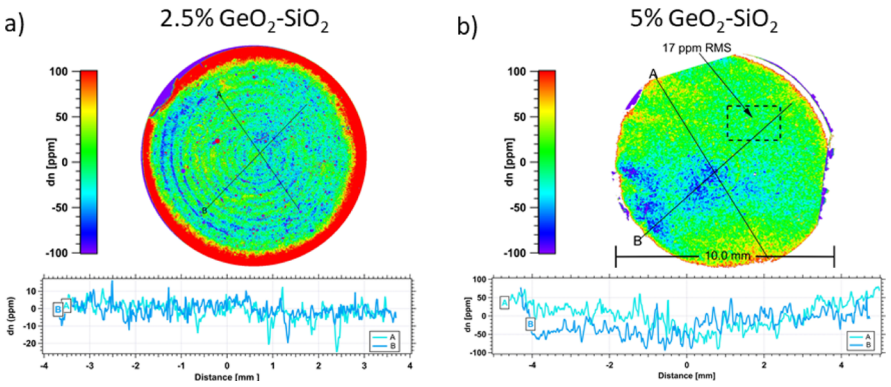

Figure 7. Optical interferometric characterization of (a) 2.5% GeO_2−SiO_2 and (b) 5% GeO_2−SiO_2 DIW, 3D printed glasses. Both data sets: (a,b) refractive index variation image (top) and respective profile line plots (bottom).

consistent with that observed in GeO_2−SiO_2 binary glass fabricated by conventional methods (i.e., sol−gel and melting).[31,32] For comparison, 3D printed TiO_2−SiO_2 glasses have an Abbe number of ∼50.[3] Therefore, the DIW GeO_2−SiO_2 glasses offer the prospect of producing a higher index 3D printed glass with both improved UV performance and reduced dispersion compared to Ti-doped silica glasses.

Of significant concern in developing 3D printed glasses for optics are the presence of localized regions of nonuniform concentration or defects generated at the interfaces, both of which translate into refractive index inhomogeneity and result in optical losses. Figure 7a,b shows the map of refractive index homogeneity for printed 2.5 and 5% GeO_2−SiO_2 glasses, respectively, measured via transmission interferometry. Figure 7a shows that 2.5% GeO_2−SiO_2 exhibits very high refractive index homogeneity with print lines that are faintly visible. The associated profile lines show that the standard deviation is extremely low at less than 5 ppm.[3] This low level of variation is sufficient for many optical applications. Figure 7b shows that 5% GeO_2−SiO_2 has an index homogeneity of approximately 17 ppm, with little evidence of print lines. Although the index variation is higher than that of the 2.5% GeO_2−SiO_2 glass, it is still within specification for many optical applications.[3]

4. CONCLUSIONS

Germania−silicate glasses with high optical transparency and high index homogeneity have been prepared for the first time via 3D printing. Printable inks with desired rheological characteristics were obtained by mixing separate sol−gel-derived nanoparticles of GeO_2 and SiO_2 in low vapor pressure organic solvents. These inks were then printed via DIW and heat-treated to form fully dense, transparent glasses. Chemical and structural evolutions were confirmed by NMR, XRD, and Raman spectroscopies. UV−vis transmission measurements showed that the optical transmissions of 2.5 and 5% GeO_2−SiO_2 glasses are comparable to that of commercial fused silica. Furthermore, optical characterization of GeO_2−SiO_2 DIW-printed glasses shows high refractive index homogeneity with little evidence of print lines and the potential for reduced chromatic aberration and better performance when compared with previously demonstrated TiO_2−SiO_2 DIW glasses. This work provides a previously unavailable glass type for preparing multimaterial DIW 3D printing and offers new possibilities for fabricating optical quality glasses which are unattainable by conventional methods. Ongoing efforts seek to expand the range of glass compositions, further increase the achievable refractive index, and create gradient index components, all of which will help establish DIW 3D printing as an alternative manufacturing methodology for novel optical components.

■ ASSOCIATED CONTENT

Supporting Information

The Supporting Information is available free of charge at https://pubs.acs.org/doi/10.1021/acsami.9b21136.

Experimental details, heat treatment protocol, NMR, thermogravimetric analysis, dynamic light scattering, EMPA, UV−vis, and rheology measurements (PDF)

■ AUTHOR INFORMATION

Corresponding Author

Koroush Sasan − *Lawrence Livermore National Laboratory, Livermore, California 94550, United States;* orcid.org/0000-0002-5577-8894; Email: sasan2@llnl.gov

Authors

Andrew Lange − *Lawrence Livermore National Laboratory, Livermore, California 94550, United States;* orcid.org/0000-0002-6762-0736

Timothy D. Yee − *Lawrence Livermore National Laboratory, Livermore, California 94550, United States*

Nikola Dudukovic − *Lawrence Livermore National Laboratory, Livermore, California 94550, United States;* orcid.org/0000-0002-0852-7080

Du T. Nguyen − *Lawrence Livermore National Laboratory, Livermore, California 94550, United States;* orcid.org/0000-0001-5509-3345

Michael A. Johnson − *Lawrence Livermore National Laboratory, Livermore, California 94550, United States*

Oscar D. Herrera − *Lawrence Livermore National Laboratory, Livermore, California 94550, United States*

Jae Hyuck Yoo − *Lawrence Livermore National Laboratory, Livermore, California 94550, United States;* orcid.org/0000-0002-7270-1688

April M. Sawvel − *Lawrence Livermore National Laboratory, Livermore, California 94550, United States;* orcid.org/0000-0002-8810-807X

Megan Elizabeth Ellis − *Lawrence Livermore National Laboratory, Livermore, California 94550, United States*

Christopher M. Mah − *Lawrence Livermore National Laboratory, Livermore, California 94550, United States*

Rick Ryerson − *Lawrence Livermore National Laboratory, Livermore, California 94550, United States*

https://dx.doi.org/10.1021/acsami.9b21136
ACS Appl. Mater. Interfaces 2020, 12, 6736−6741

Lana L. Wong − *Lawrence Livermore National Laboratory, Livermore, California 94550, United States*
Tayyab Suratwala − *Lawrence Livermore National Laboratory, Livermore, California 94550, United States*
Joel F. Destino − *Creighton University, Omaha, Nebraska 68178, United States*
Rebecca Dylla-Spears − *Lawrence Livermore National Laboratory, Livermore, California 94550, United States*

Complete contact information is available at: https://pubs.acs.org/10.1021/acsami.9b21136

Notes

The authors declare no competing financial interest.

■ ACKNOWLEDGMENTS

This work was performed under the auspices of the U.S. Department of Energy by the Lawrence Livermore National Laboratory under Contract DE-AC52-07NA27344 within the LDRD program 19-ERD-020. LLNL-JRNL-770218.

■ REFERENCES

(1) Cooperstein, I.; Shukrun, E.; Press, O.; Kamyshny, A.; Magdassi, S. Additive Manufacturing of Transparent Silica Glass from Solutions. *ACS Appl. Mater. Interfaces* **2018**, *10*, 18879−18885.
(2) Ikushima, A. J.; Fujiwara, T.; Saito, K. Silica Glass: A Material for Photonics. *J. Appl. Phys.* **2000**, *88*, 1201−1213.
(3) Destino, J. F.; Dudukovic, N. A.; Johnson, M. A.; Nguyen, D. T.; Yee, T. D.; Egan, G. C.; Sawvel, A. M.; Steele, W. A.; Baumann, T. F.; Duoss, E. B.; Suratwala, T.; Dylla-Spears, R. 3D Printed Optical Quality Silica and Silica−titania Glasses from Sol−gel Feedstocks. *Adv. Mater. Technol.* **2018**, *3*, 1700323.
(4) Luo, J.; Smith, N. J.; Pantano, C. G.; Kim, S. H. Complex Refractive Index of Silica, Silicate, Borosilicate, and Boroaluminosilicate Glasses−Analysis of Glass Network Vibration Modes with Specular-reflection IR Spectroscopy. *J. Non-Cryst. Solids* **2018**, *494*, 94−103.
(5) Kang, M.; Sisken, L.; Cook, J.; Blanco, C.; Richardson, M. C.; Mingareev, I.; Richardson, K. Refractive Index Patterning of Infrared Glass Ceramics through Laser-induced Vitrification. *Opt. Mater. Express* **2018**, *8*, 2722−2733.
(6) Klein, J.; Stern, M.; Franchin, G.; Kayser, M.; Inamura, C.; Dave, S.; Weaver, J. C.; Houk, P.; Colombo, P.; Yang, M.; Oxman, N. Additive Manufacturing of Optically Transparent Glass. *3D Print. Addit. Manuf.* **2015**, *2*, 92−105.
(7) Neustruev, V. B. Colour Centres in Germanosilicate Glass and Optical Fibres. *J. Phys.: Condens. Matter* **1994**, *6*, 6901−6936.
(8) Uchino, T.; Nakaguchi, K.; Nagashima, Y.; Kondo, T. Prediction of Optical Properties of Commercial Soda−lime-silicate Glasses Containing Iron. *J. Non-Cryst. Solids* **2000**, *261*, 72−78.
(9) Bauer, J.; Schroer, A.; Schwaiger, R.; Kraft, O. Approaching Theoretical Strength in Glassy Carbon Nanolattices. *Nat. Mater.* **2016**, *15*, 438−443.
(10) Dudukovic, N. A.; Wong, L. L.; Nguyen, D. T.; Destino, J. F.; Yee, T. D.; Ryerson, F. J.; Suratwala, T.; Duoss, E. B.; Dylla-Spears, R. Predicting Nanoparticle Suspension Viscoelasticity for Multimaterial 3D Printing of Silica−Titania Glass. *ACS Appl. Nano Mater.* **2018**, *1*, 4038−4044.
(11) Kotz, F.; Arnold, K.; Bauer, W.; Schild, D.; Keller, N.; Sachsenheimer, K.; Nargang, T. M.; Richter, C.; Helmer, D.; Rapp, B. E. Three-dimensional Printing of Transparent Fused Silica Glass. *Nature* **2017**, *544*, 337−339.
(12) Vaidya, N.; Solgaard, O. 3D Printed Optics with Nanometer Scale Surface Roughness. *Microsyst. Nanoeng.* **2018**, *4*, 18.
(13) Luo, J.; Gilbert, L. J.; Qu, C.; Landers, R. G.; Bristow, D. A.; Kinzel, E. C. Additive Manufacturing of Transparent Soda-lime Glass Using a Filament-fed Process. *J. Manuf. Sci. Eng.* **2017**, *139*, 061006.
(14) Luo, J.; Pan, H.; Kinzel, E. C. Additive Manufacturing of Glass. *J. Manuf. Sci. Eng.* **2014**, *136*, 061024.
(15) Luo, J.; Gilbert, L. J.; Bristow, D. A.; Landers, R. G.; Goldstein, J. T.; Urbas, A. M.; Kinzel, E. C. Additive Manufacturing of Glass for Optical Applications. *Laser 3D Manufacturing III*; International Society for Optics and Photonics, 2016; p 97380Y.
(16) Nguyen, D. T.; Meyers, C.; Yee, T. D.; Dudukovic, N. A.; Destino, J. F.; Zhu, C.; Duoss, E. B.; Baumann, T. F.; Suratwala, T.; Smay, J. E.; Dylla-Spears, R. 3D-Printed Transparent Glass. *Adv. Mater.* **2017**, *29*, 1701181.
(17) Nguyen, D. T.; Yee, T. D.; Dudukovic, N. A.; Sasan, K.; Jaycox, A. W.; Golobic, A. M.; Duoss, E. B.; Dylla-Spears, R. 3D Printing of Compositional Gradients Using the Microfluidic Circuit Analogy. *Adv. Mater. Technol.* **2019**, *4*, 1900784.
(18) Boulogne, F.; Giorgiutti-Dauphiné, F.; Pauchard, L. How to Reduce the Crack Density in Drying Colloidal Material? *Oil Gas Sci. Technol. -Rev. d'IFP Energ. Nouv.* **2014**, *69*, 397−404.
(19) Piroird, K.; Lazarus, V.; Gauthier, G.; Lesaine, A.; Bonamy, D.; Rountree, C. L. Role of Evaporation Rate on the Particle Organization and Crack Patterns Obtained by Drying a Colloidal Layer. *Europhys. Lett.* **2016**, *113*, 38002.
(20) Schneider, M.; Maurath, J.; Fischer, S. B.; Weiß, M.; Willenbacher, N.; Koos, E. Suppressing Crack Formation in Particulate Systems by Utilizing Capillary Forces. *ACS Appl. Mater. Interfaces* **2017**, *9*, 11095−11105.
(21) Drummond, C. H.; Turnbull, D. Phase Separation in Ge-GeO_2 Glasses. *J. Non-Cryst. Solids* **1975**, *17*, 19−26.
(22) Shaw, R. R.; Uhlmann, D. R. Effect of Phase Separation on the Properties of Simple Glasses I. Density and Molar Volume. *J. Non-Cryst. Solids* **1969**, *1*, 474−498.
(23) Minke, M. V.; Jackson, K. A. Diffusion of Germanium in Silica Glass. *J. Non-Cryst. Solids* **2005**, *351*, 2310−2316.
(24) Wang, P. W.; Feng, Y. P.; Roth, W. L.; Corbett, J. W. Diffusion Behavior of Implanted Iron in Fused Silica Glass. *J. Non-Cryst. Solids* **1988**, *104*, 81−84.
(25) van Ommen, A. H. Diffusion of Ion-implanted Ga in SiO_2. *J. Appl. Phys.* **1985**, *57*, 1872−1879.
(26) van Ommen, A. H. Diffusion of ion-implanted In and Tl in SiO_2. *J. Appl. Phys.* **1985**, *57*, 5220−5225.
(27) Chen, D.-G.; Potter, B. G.; Simmons, J. H. GeO_2-SiO_2 Thin Films for Planar Waveguide Applications. *J. Non-Cryst. Solids* **1994**, *178*, 135−147.
(28) Sharma, S. K.; Matson, D. W.; Philpotts, J. A.; Roush, T. L. Raman Study of the Structure of Glasses Along the Join SiO_2-GeO_2. *J. Non-Cryst. Solids* **1984**, *68*, 99−114.
(29) Henderson, G. S.; Neuville, D. R.; Cochain, B.; Cormier, L. The structure of GeO_2−SiO_2 glasses and melts: A Raman spectroscopy study. *J. Non-Cryst. Solids* **2009**, *355*, 468−474.
(30) Mukherjee, S. P.; Sharma, S. K. A comparative Raman Study of the Structures of Conventional and Gel-derived Glasses in the SiO_2-GeO_2 System. *J. Non-Cryst. Solids* **1985**, *71*, 317−325.
(31) Fleming, J. W. Dispersion in GeO_2−SiO_2 Glasses. *Appl. Opt.* **1984**, *23*, 4486−4493.
(32) Huang, Y. Y.; Sarkar, A.; Schultz, P. C. Relationship Between Composition, Density and Refractive Index for Germania Silica Glasses. *J. Non-Cryst. Solids* **1978**, *27*, 29−37.